

Clinical Utility of Dual-Energy CT in the Evaluation of Solitary Pulmonary Nodules: Initial Experience¹

Eun Jin Chae, MD
Jae-Woo Song, MD, PhD
Joon Beom Seo, MD, PhD
Bernhard Krauss, PhD
Yu Mi Jang, MD
Koun-Sik Song, MD, PhD

Purpose:

To determine the clinical utility of dual-energy computed tomography (CT) in evaluating solitary pulmonary nodules (SPNs).

Materials and Methods:

This study was approved by the institutional review board, and informed consent was obtained. CT scans were obtained before and 3 minutes after contrast material injection in 49 patients (26 men, 23 women; mean age, 60.39 years \pm 12.24 [standard deviation]) by using a scanner with a dual-energy technique. Image sets that included nonenhanced weighted average, enhanced weighted average, virtual nonenhanced, and iodine-enhanced images were reconstructed. CT numbers of SPNs on virtual nonenhanced and nonenhanced weighted average images were compared, and CT numbers on iodine-enhanced image and the degree of enhancement were compared. Diagnostic accuracy for malignancy by using CT number on iodine-enhanced image and the degree of enhancement were compared. On the virtual nonenhanced image, the number and size of calcifications were compared with those on the nonenhanced weighted average image. Radiation dose was compared with that of single-energy CT.

Results:

CT numbers on virtual nonenhanced and nonenhanced weighted average images and CT numbers on the iodine-enhanced image and the degree of enhancement showed good agreements (intraclass correlation coefficients: 0.83 and 0.91, respectively). Diagnostic accuracy for malignancy by using CT numbers on iodine-enhanced image was comparable to that by using the degree of enhancement (sensitivity, 92% and 72%; specificity, 70% and 70%; accuracy, 82.2% and 71.1%, respectively). On virtual nonenhanced image, 85.0% (17 of 20) of calcifications in the SPN and 97.8% (44 of 45) of calcifications in the lymph nodes were detected, and the apparent sizes were smaller than those on the nonenhanced weighted average image. Radiation dose (average dose-length product, 240.77 mGy \cdot cm) was not significantly different from that of single-energy CT ($P = .67$).

Conclusion:

Dual-energy CT allows measurement of the degree of enhancement and detection of calcifications without additional radiation dose.

© RSNA, 2008

¹ From the Department of Radiology and Research Institute of Radiology, University of Ulsan College of Medicine, Asan Medical Center, 388-1, Poongnap-dong, Songpa-gu, Seoul 138-736, Korea (E.J.C., J.W.S., J.B.S., Y.M.J., K.S.S.); and Siemens Medical Solutions, Forchheim, Germany (B.K.). Received November 9, 2007; revision requested January 14, 2008; revision received April 5; accepted April 17; final version accepted May 29. Supported by a grant (2007-439) from the Asan Institute for Life Sciences, Seoul, Korea. Address correspondence to J.W.S. (e-mail: jwsong49@amc.seoul.kr).

The dual-energy (DE) technique of a dual-source computed tomographic (CT) scanner allows differentiation of iodine from other materials due to its stronger photoelectric absorption. CT numbers vary noticeably with beam energy for materials having a high atomic number, but much less for other materials. Therefore, materials can be differentiated by applying different x-ray spectra and analyzing the differences in attenuation (1). One potential application of iodine differentiation with the DE technique is to differentiate contrast material-enhanced structures from the otherwise dense material in parenchymatous organs, for example, to differentiate complicated cysts from neoplastic tissue in the kidney (1,2). To differentiate calcification from enhancing tissue in a solitary pulmonary nodule (SPN) or in the mediastinal lymph node is another potential application.

Chest CT is usually performed as a combination of nonenhanced and enhanced scanning. A nonenhanced scan is obtained for the detection of calcification in the SPN or in the lymph node, since the presence of calcification is one of the important deterministic findings of benignity. An enhanced scan is informative in providing the degree and pattern of enhancement with use of iodine. In particular, the degree of enhancement of an SPN

after iodine injection has proved to be helpful for distinguishing malignant from benign nodules (3–9). Application of the DE technique provides a virtual nonenhanced and an iodine-enhanced image from a single scanning after iodine contrast material injection by material differentiation of iodine. If we are able to detect calcification on a virtual nonenhanced image and directly measure the iodine component on an iodine-enhanced image, this technique may prevent additional nonenhanced scanning and the patient's radiation exposure will then be reduced. The purpose of our study was to assess the potential clinical utility of DE CT in evaluating an SPN in the detectability of calcification, measurement of the degree of enhancement, and comparison of the radiation dose.

Materials and Methods

A prototype of a commercial software product Syngo Dual Energy (Siemens Medical Solutions) was used for data analysis. B.K. has played a role in data acquisition and analysis in terms of modification of parameters of dedicated dual-energy software and interpretation of acquired CT data.

Subjects

This research protocol was approved by the institutional review board of our institution, and written informed consent was obtained from all patients. From January 2007 to July 2007, a total of 49 patients (26 men, 23 women; age range, 31–80 years; mean age, 60.39 years \pm 12.24 [standard deviation]) who were scheduled to undergo percutaneous needle aspiration of an SPN were consecutively enrolled.

Implications for Patient Care

- DE CT allows measurement of the degree of enhancement of lung nodules, as well as the detection of calcifications in the lung nodules and lymph nodes.
- By single scanning after iodine injection with DE CT, we may measure the degree of enhancement without an additional non-enhanced scan.

CT Examination

CT examinations were performed by using the DE mode of the Somatom Definition scanner (Siemens Medical Solutions, Forchheim, Germany) with a 512×512 -pixel matrix, 14×1.2 -mm collimation, 50 mAs (effective) at 140 kV and 210 mAs (effective) at 80 kV, pitch of 0.7, and rotation time of 0.5 second. We used a dedicated DE CT protocol for the thorax, which was recommended by the manufacturer. Tube currents of two x-ray tubes of 80 kV and 140 kV were fixed as ratio of approximately 4:1 (50 mAs [effective] for 80 kV and 210 mAs [effective] for 140 kV). Each tube has 24 rows of 1.2 mm; however, only some of them were used (14×1.2 mm) to allow for an improved scatter-correction by using the outer rows. The craniocaudal direction was used for all scans. In patients ($n = 25$) who had previously undergone a conventional chest CT before the procedure, the targeted CT scans covering the SPN were obtained both before (nonenhanced scan) and 3 minutes after contrast material injection (3-minute-delayed scan) for this study (protocol 1) (Fig 1). A 100 mL of iomeprol (Iomeron 300; Bracco, Milan, Italy) was administered at a rate of 3.0 mL/sec by using a power injector. In patients ($n = 24$)

Advances in Knowledge

- Dual-energy (DE) CT can provide both virtual nonenhanced and iodine-enhanced images from a single scanning after iodine injection.
- DE CT allows differentiation of calcification from enhancing tissue by subtraction of the iodine component according to the material decomposition theory.
- The iodine component in lung nodules is measurable on iodine-enhanced image and is comparable to the real value of the degree of enhancement.
- The radiation dose of a single scanning covering the full thorax using DE CT is not significantly different from that using single-energy CT.

Published online before print

10.1148/radiol.2492071956

Radiology 2008; 249:671–681

Abbreviations:

CI = confidence interval
 DE = dual energy
 ICC = intraclass correlation coefficient
 ROI = region of interest
 SPN = solitary pulmonary nodule

Author contributions:

Guarantor of integrity of entire study, J.W.S.; study concepts/study design or data acquisition or data analysis/interpretation, all authors; manuscript drafting or manuscript revision for important intellectual content, all authors; approval of final version of submitted manuscript, all authors; literature research, E.J.C., J.W.S., J.B.S., Y.M.J., K.S.S.; clinical studies, E.J.C., J.W.S., J.B.S., Y.M.J., K.S.S.; statistical analysis, E.J.C., J.W.S., J.B.S., K.S.S.; and manuscript editing, E.J.C., J.W.S., J.B.S., B.K., K.S.S.

See Materials and Methods for pertinent disclosures.

who had not previously undergone chest CT for the evaluation of an SPN, a 1-minute-delayed scan covering the full thorax was acquired for routine clinical practice in addition to the protocol 1 scan (protocol 2) (Fig 1). For all patients, data of 80 kV, 140 kV, and weighted average image of nonenhanced and 3-minute-delayed scans targeted for SPN were transferred to a workstation (MultiModality Workplace; Siemens Medical Solutions). The weighted average image is the approximate 120-kV image, which is automatically generated from a combination of 140-kV and 80-kV data by using weighting factor 1:4 (140 kV: 80 kV). In protocol 2 patients, weighted average images of 1-minute-delayed scan were transferred to a picture archiving and communication system workstation for clinical use.

Material Decomposition

By using two acquisition systems of the dual-source CT, both x-ray tubes can be operated at different kilovoltage settings, allowing the acquisition of DE data. The DE technique allows differentiation and extraction of iodine from the enhanced soft tissue on the basis of the material decomposition theory (10,11). Iodine leads to a very large difference between the 80-kV and the 140-kV image. A diagram shows the CT value at 80 kV versus 140 kV, and iodine enhancement is represented by a vector of fixed direction but the length depends on iodine attenuation (Fig 2). As for these spectra, the typical body materials such as fat, water, soft tissue, and liver tissue are approximately located on a straight line in this diagram; a two-dimensional linear equation can be solved to obtain the attenuation coefficient (in Hounsfield units) due to iodine (iodine-enhanced image) and an image that contains only the contribution of the body materials (virtual nonenhanced image) (12).

Data Analysis

Image data were reconstructed with a section thickness of 2.0 mm by using kernel D30 and an increment of 2.0 mm. By using a modified prototype of

the Liver VNC application class of Syngo Dual Energy (Siemens Medical Solutions) on a dedicated research MultiModality Workplace workstation, virtual nonenhanced and iodine-enhanced images were calculated from the 3-minute-

delayed scan data. The commercially available software was modified to allow for negative CT numbers on the iodine image, which improves region-of-interest (ROI) measurements of very low concentrations of contrast material.

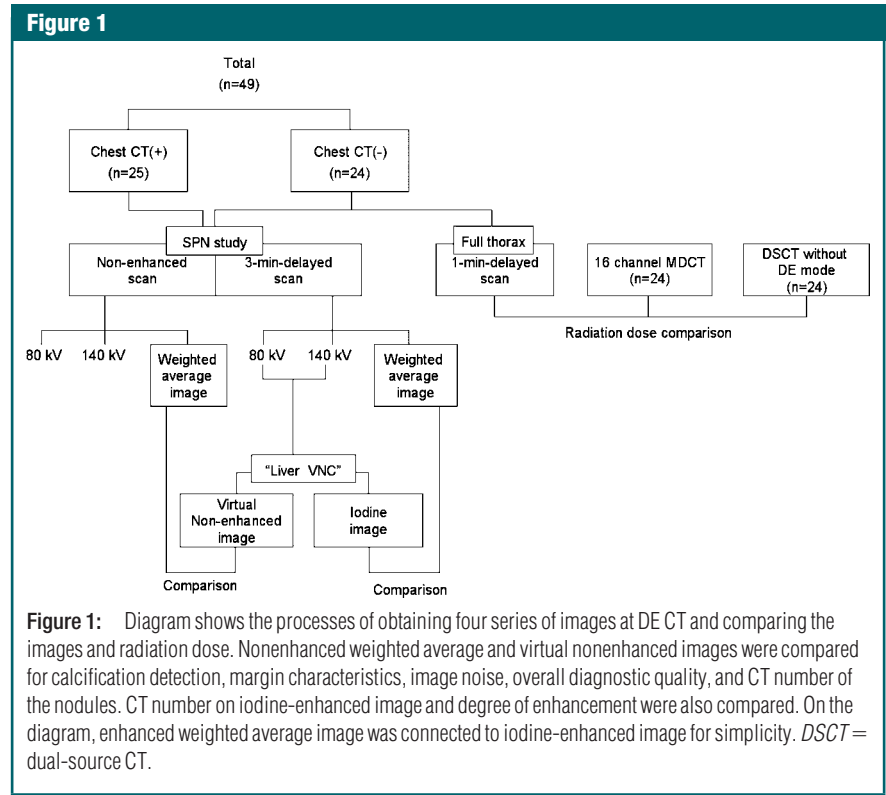


Figure 1: Diagram shows the processes of obtaining four series of images at DE CT and comparing the images and radiation dose. Nonenhanced weighted average and virtual nonenhanced images were compared for calcification detection, margin characteristics, image noise, overall diagnostic quality, and CT number of the nodules. CT number on iodine-enhanced image and degree of enhancement were also compared. On the diagram, enhanced weighted average image was connected to iodine-enhanced image for simplicity. DSCT = dual-source CT.

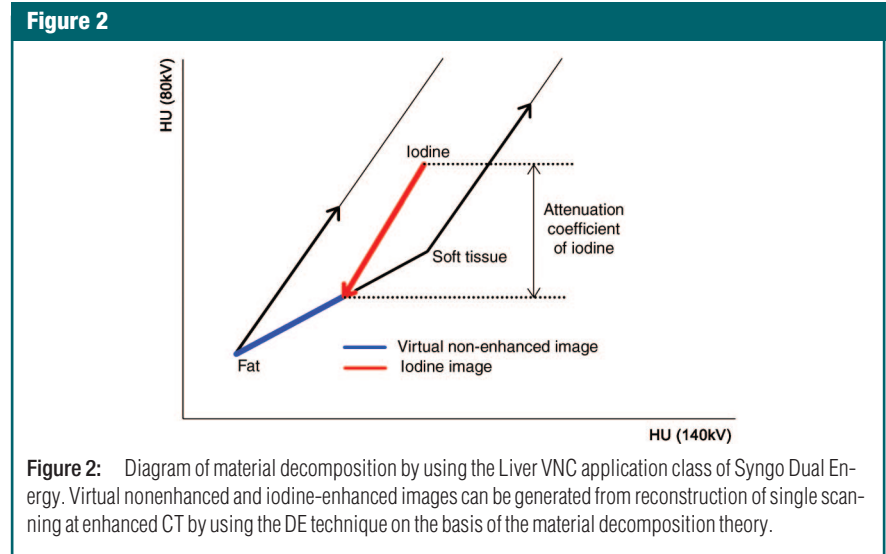


Figure 2: Diagram of material decomposition by using the Liver VNC application class of Syngo Dual Energy. Virtual nonenhanced and iodine-enhanced images can be generated from reconstruction of single scanning at enhanced CT by using the DE technique on the basis of the material decomposition theory.

The material parameters for the material decomposition method are as follows: -110 HU for fat at 80 kV, -96 HU for fat at 140 kV, 60 HU for soft tissue at 80 kV, and 54 HU for soft tissue at 140 kV. It is an empirical observation that for DE scans obtained with the Somatom Definition scanner, typical tissues inside the human body are approximately located on this line in the 80-kV versus the 140-kV diagram of the Hounsfield units; this includes fat and liver parenchyma, as well as blood, muscle, or water (a similar behavior can be seen in published results [13] with a different scanner and the voltage combination of 100 kV/140 kV). This is also valid for mixtures of these materials on a macroscopic or microscopic scale, which seems to apply for lung nodules.

A value of 2.0 was chosen for relative contrast material enhancement, which means that the iodine enhancement at 80 kV is twice the value at 140 kV. Material decomposition was only performed for voxels with Hounsfield units in the mixed image between -300 HU (minimum value) and $+300$ HU (maximum value) (14). The parameter “range,” which controls the size of the spherical three-dimensional filter kernel in units of the voxel size, was set to 2. The maximum value was adjusted to 300 from 3071 of the default value because we intended to differentiate between dense calcifications and the iodine component. The iodine component was demonstrated as a color overlay on a background virtual nonenhanced image of 3-minute-delayed scan with semi-transparent mode (Fig 3). For each patient, four image series that included a nonenhanced weighted average image, enhanced weighted average image, virtual nonenhanced image, and iodine-enhanced image were obtained (Fig 1).

Detectability of Calcification on Virtual Nonenhanced Image

On virtual nonenhanced image, the number and size of calcifications within the SPN and lymph nodes were compared with those on nonenhanced weighted average image. A chest radiologist with 5 years of experience performed all visual assessments, including detection of calcifi-

cation. Biopsy was performed on all detected calcifications within the nodule, other lung nodules within scan range and lymph nodes within scan range were counted. The number of detected calcifications was scored on both virtual nonenhanced and nonenhanced weighted average images. The calcification size on virtual nonenhanced image was compared with that on nonenhanced weighted average image according to following grades: grade 1, the same; grade 2, smaller; grade 3, nonvisualized; and grade 4, new calcific attenuation. On enhanced weighted average image, the number of detected calcifications was also recorded to determine how many obscured calcifications on enhanced weighted average image appear on virtual nonenhanced image.

The subjective evaluation of the margin characteristics of an SPN, the image noise, and the overall diagnostic quality of both virtual nonenhanced and nonenhanced weighted average images was performed and compared with each other. For margin characteristics, grade 1 = smooth; grade 2 = lobulated; grade 3 = irregular; and grade 4 = spiculated. For the image noise of virtual nonenhanced image, grade 1 = lower; grade 2 = the same; and grade 3, greater. For the diagnostic quality of virtual nonenhanced image, grade 1 = superior; grade 2 = the same; grade 3 = poor, but diagnostic; and grade 4 = unacceptable.

We measured the chest diameter and recorded the location of the nodules in all patients to assess the effect of size of the small detector system. The location of the nodules was described as central, middle, or peripheral.

Comparison of the CT Number between Virtual and Real Images

A chest radiologist with 5 years of experience placed a circular ROI in as large an area as possible within the SPN. Image data of the nonenhanced and the 3-minute-delayed scans targeted for SPN were loaded on the “dual energy” tab of the Syngo Dual-Energy application of the MultiModality Workplace workstation. Because two series could not be loaded simultaneously, two ROIs

were used to measure the nonenhanced and the 3-minute-delayed scans. To assess whether differentiation of iodine was successful, the CT numbers of SPN on virtual nonenhanced and nonenhanced weighted average images, as well as CT numbers of the SPN on iodine-enhanced image and the degree of enhancement (CT number on enhanced weighted average image $-$ CT number on nonenhanced weighted average image), were compared. The sum of the CT number of SPN on iodine-enhanced image and virtual nonenhanced image was compared with the CT number on enhanced weighted average image. The CT numbers of the SPN on iodine-enhanced image and the degree of enhancement were compared in terms of their diagnostic accuracy for distinguishing malignant and benign nodules with a 20-HU threshold. We selected a 20 HU as a cutoff value on the basis of results of previous studies (3–6).

Radiation Dose

The radiation doses of protocol 1 (both nonenhanced and 3-minute-delayed scans targeted for SPN, $n = 25$) and protocol 2 (protocol 1 plus 1-minute-delayed scan covering full thorax, $n = 24$) in all patients were recorded as the value of the dose-length product. Dose parameters were obtained from the “Patient Protocol” image (Siemens Medical Solutions), which is an image file that includes the information of the CT protocol and the amount of radiation dose. That image is automatically exported to picture archiving and communication system workstation with other CT images. Dose-length product of the 1-minute-delayed scan covering the full thorax in 24 patients was used for comparison with other examinations using single-energy CT. The radiation dose was recorded in 24 CT examinations with 16-detector CT (Somatom Sensation 16, Siemens Medical Solutions) and in 24 examinations with dual-source CT without applying the DE mode. Without the DE mode, only the A system operates; therefore, this works as same as the 64-detector CT. Those 48 CT examinations were randomly selected among all the CT examinations performed on 3

consecutive days in our institution. The radiation doses of multidetector CT, dual-source CT, and DE CT were then compared.

Statistical Analysis

Commercial statistical packages (version 12.1.1 SPSS, Chicago, Ill; and version 7.3, MedCalc Software, Mariakerke, Belgium) were used. The results were expressed as mean \pm

standard deviation. Descriptive statistics were used to evaluate the number and size of the calcifications, image noise, and overall diagnostic quality. Agreement of the margin characteristics of SPN between virtual nonenhanced image and nonenhanced weighted average image was analyzed with κ statistics. Agreement in the CT numbers of SPN on four image series was analyzed by calculating the intraclass correlation co-

efficient (ICC) and using the Bland-Altman method. The Mann-Whitney *U* test was used to analyze statistically significant differences between the CT numbers of benign and malignant nodules. Between the CT number on iodine-enhanced image and the degree of enhancement, the diagnostic accuracy was compared by calculating the sensitivity, specificity, and accuracy with 95% confidence intervals (CIs) (15). The Mann-

Figure 3

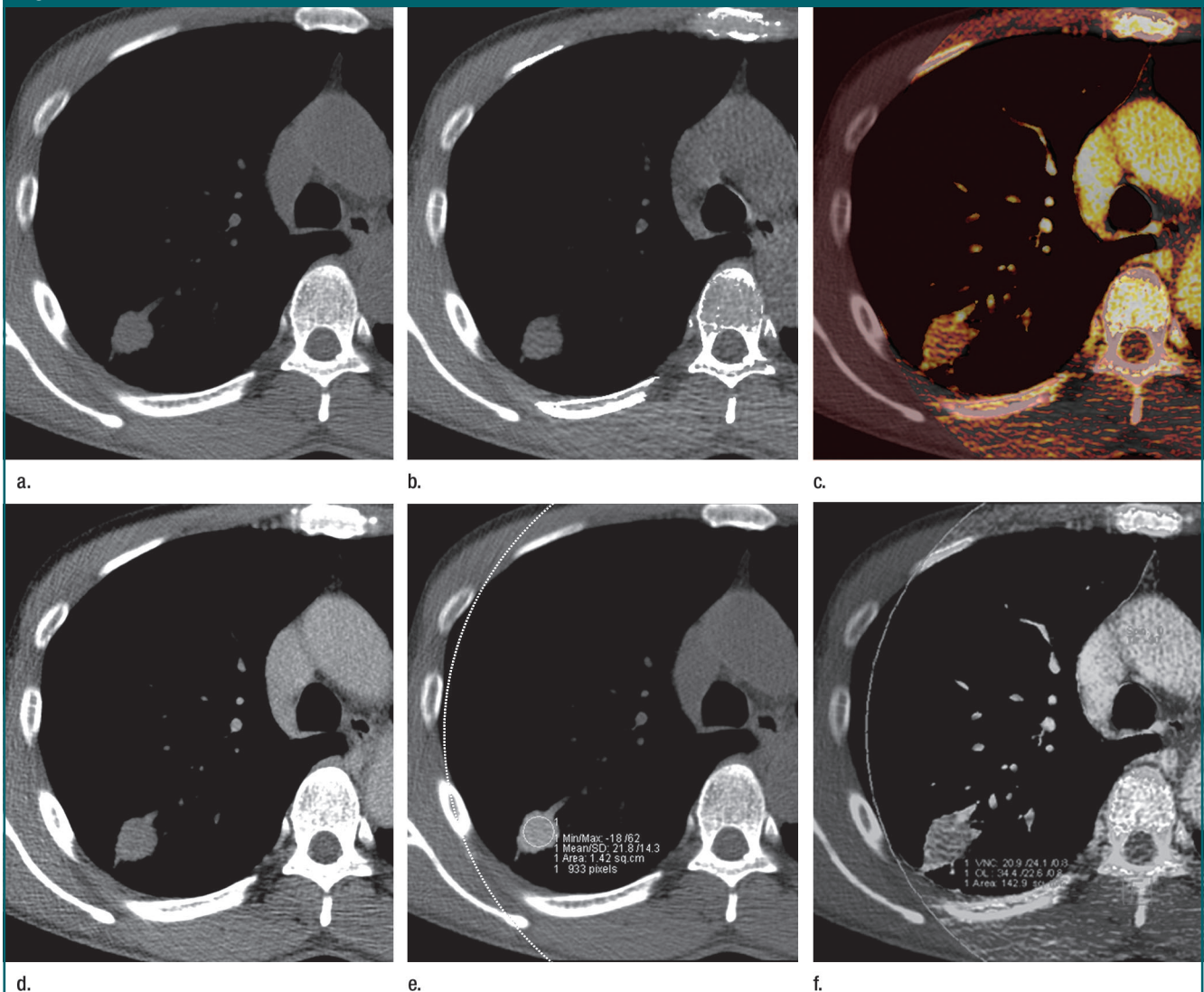


Figure 3: Images in 57-year-old man with a nodule. (a) Nonenhanced weighted average image. (b) Virtual nonenhanced image. (c) Iodine-enhanced image. The iodine component was demonstrated as a color overlay in the semitransparent mode. (d) Enhanced weighted average image. (e) Nonenhanced weighted average image shows an ROI in the nodule with a CT number of 21.8 HU. (f) VNC of ROI represents the CT number on background virtual nonenhanced image and OL represents the CT number on iodine-enhanced image, which indicates the iodine component in the nodule. The CT number (20.9 HU) of VNC approximates the CT number (21.8 HU) of the nodule on nonenhanced weighted average image. A circle represents the field of view of the smaller detector system.

Whitney U-test was used to compare the radiation dose among the CT examinations. A *P* value of less than .05 was considered to indicate a significant difference, and all *P* values were two tailed.

Results

The size of SPNs ranged from 5 to 70 mm, and the average size was 24.8 mm in diameter \pm 11.8. The average ROI was 705.7 pixels \pm 962.2 and 1.58 cm² \pm 2.3. The average maximum chest diameter of our patients was 304.56

mm \pm 25.11. Among the central, middle, and peripheral nodule locations, 11 nodules were located within the periphery.

Detectability of Calcification on Virtual Nonenhanced Image

On nonenhanced weighted average image, 20 calcifications were present in the nodules of four patients and 45 calcifications were present in the lymph nodes of 11 patients (Figs 4 and 5). On virtual nonenhanced image, 85.0% (17 of 20) of calcifications in the nodules and 97.8% (44 of 45) of calcifications in

the lymph nodes were detected. On virtual nonenhanced image, the sizes of the calcifications were smaller than those on nonenhanced weighted average image in all patients with calcification (*n* = 14).

The margin characteristics between virtual nonenhanced image and nonenhanced weighted average image showed a strong agreement (weighted κ in the quadratic set, 0.91; standard error, 0.14). Virtual nonenhanced image had the same degree of noise in 16.3% (eight of 49) of our patients and more noise in 83.7% (41 of 49) of these pa-

Figure 4

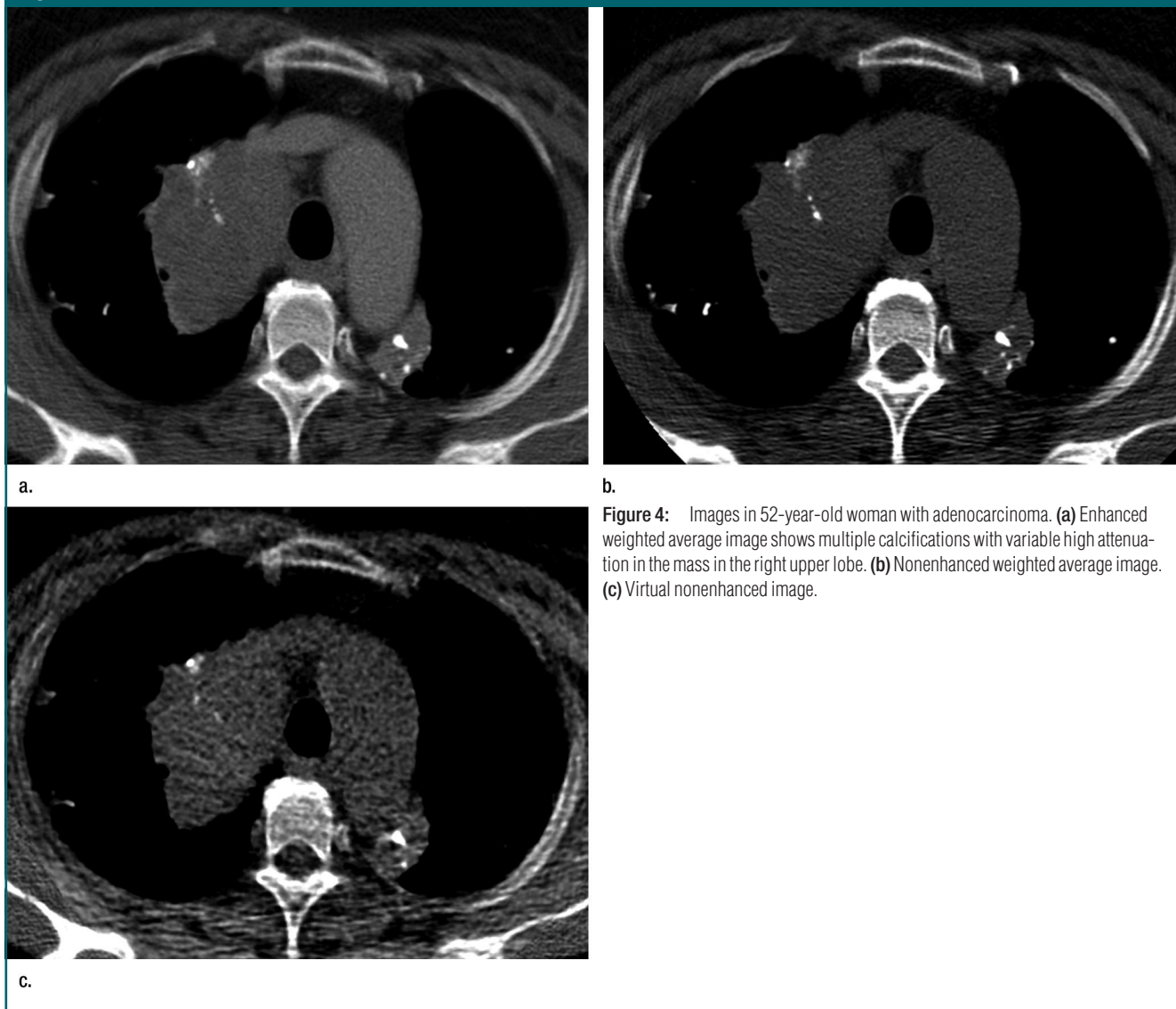


Figure 4: Images in 52-year-old woman with adenocarcinoma. (a) Enhanced weighted average image shows multiple calcifications with variable high attenuation in the mass in the right upper lobe. (b) Nonenhanced weighted average image. (c) Virtual nonenhanced image.

Figure 5



Figure 5: Depiction of calcification in the mediastinal lymph nodes. **(a)** Nonenhanced weighted average image shows two calcifications in the right lower paratracheal nodal station. **(b)** Virtual nonenhanced image shows two calcifications in the lymph node. The size of calcifications was smaller on this image. **(c)** Enhanced weighted average image.

tients. Virtual nonenhanced image had the same diagnostic quality in 77.6% (38 of 49) of patients, inferior but diagnostic quality in 16.3% (eight of 49), and unacceptable quality in 8.2% (four of 49). In eight patients, inferior but acceptable diagnostic image quality was caused by decreased grading of the margin characteristics. The unacceptable diagnostic image quality in four patients occurred because the number of detected calcifications on virtual nonenhanced image was lower than that on nonenhanced weighted average image. In two patients, four calcifications that were obscured on enhanced weighted average image were depicted on virtual nonenhanced image (Fig 6).

Comparison of the CT Number on Virtual and Real Images

CT numbers of SPN on nonenhanced weighted average and virtual nonenhanced images showed good agreement (ICC, 0.83; $P < .001$). The CT number of SPN on iodine-enhanced image and the degree of enhancement (CT number on enhanced weighted average image minus CT number on nonenhanced weighted average image) also showed good agreement (ICC, 0.91; $P < .001$). The sum of the CT numbers of SPN on

iodine-enhanced image and virtual nonenhanced image showed a strong agreement with that on enhanced weighted average image (ICC, 0.98; $P < .001$). Results of the Bland-Altman method of the agreement of CT numbers of SPN on nonenhanced weighted average and virtual nonenhanced images, as well as the CT number of SPN on iodine-enhanced image and the degree of enhancement, are shown in Figure 7. The mean difference in CT numbers of SPN on nonenhanced weighted average image and virtual nonenhanced image was 4.3 HU (95% CI: -14.6 HU, 23.3 HU), while it was -0.5 HU (95% CI: -17.6 HU, 16.5 HU) between CT number of SPN on iodine-enhanced image and the degree of enhancement. The mean difference in CT numbers on enhanced weighted average image and the sum of CT numbers on iodine-enhanced image and virtual nonenhanced image was 3.8 HU (95% CI: -5.3 HU, 12.9 HU).

A total of 45 of 49 nodules were confirmed as benign or malignant on the basis of percutaneous needle aspiration findings, and four nodules were not confirmatively diagnosed. The prevalence of malignancy was 55.6% (25 of 45 nodules), and diagnoses included adenocarcinoma ($n = 19$),

squamous cell carcinoma ($n = 2$), metastasis ($n = 2$), lymphoma ($n = 1$), and large cell neuroendocrine cell carcinoma ($n = 1$). Diagnoses of benign nodules included tuberculosis ($n = 7$), hamartoma ($n = 3$), sclerosing hemangioma ($n = 2$), abscess ($n = 1$), aspergilloma ($n = 1$), calcified granuloma ($n = 1$), and a nonspecific inflammatory lesion ($n = 5$). Any nondiagnostic result such as insufficient specimen was not present.

The results of both the CT number on iodine-enhanced image and the degree of enhancement showed that malignant nodules enhance significantly more than do benign nodules ($P = .001$ for iodine image; $P < .001$ for degree of enhancement) (Table 1). By comparing the diagnostic accuracy with a cutoff value of 20 HU for malignant nodules, the CT number of SPN on iodine-enhanced image had higher sensitivity and accuracy than did the number using the degree of enhancement (Table 2).

Radiation Dose

CT examinations using protocol 1 were performed in 25 patients and those using protocol 2 were performed in 24 patients. The average dose-length product was $92.77 \text{ mGy} \cdot \text{cm} \pm 32.37$ in pro-

protocol 1 and $333.54 \text{ mGy} \cdot \text{cm} \pm 53.93$ in protocol 2. The average dose-length product of 1-minute-delayed scan covering the full thorax in protocol 2 was $240.77 \text{ mGy} \cdot \text{cm} \pm 37.18$. This was not significantly different from the average dose-length product of CT examinations performed by using single-energy multi-detector CT and dual-source CT without

the application of the DE mode ($235.38 \text{ mGy} \cdot \text{cm} \pm 35.40$ and $233.13 \text{ mGy} \cdot \text{cm} \pm 67.36$, respectively) ($P = .67$ and $.39$, respectively).

Discussion

On the basis of our study findings, we ascertained that the iodine component

could be successfully differentiated from the enhanced soft tissue at enhanced CT using DE. CT numbers on nonenhanced weighted average image and virtual nonenhanced image, as well as the CT number on iodine-enhanced image and the degree of enhancement, showed reliable agreement. The evaluation of tumor vascularity by measuring

Figure 6

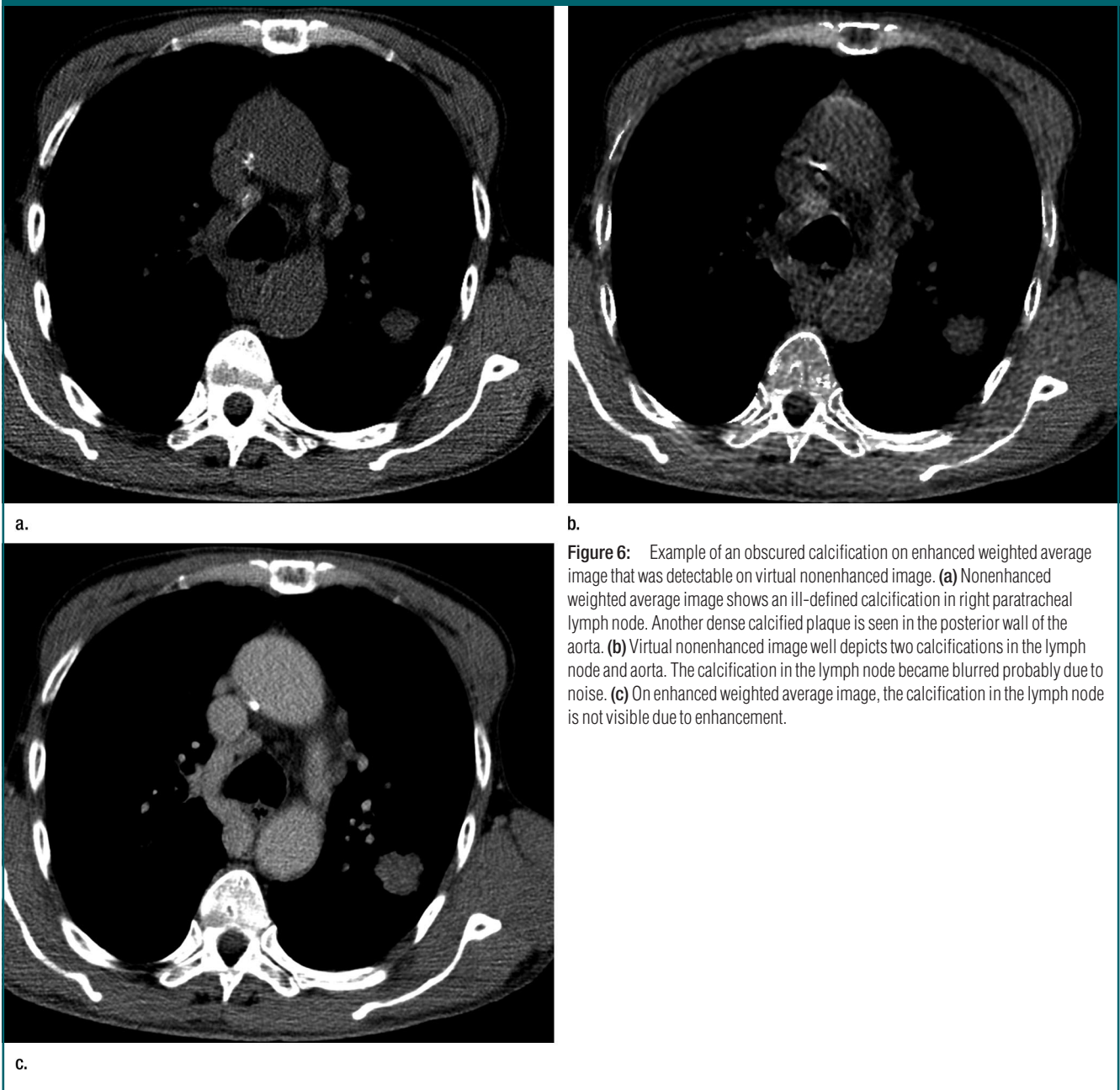


Figure 6: Example of an obscured calcification on enhanced weighted average image that was detectable on virtual nonenhanced image. **(a)** Nonenhanced weighted average image shows an ill-defined calcification in right paratracheal lymph node. Another dense calcified plaque is seen in the posterior wall of the aorta. **(b)** Virtual nonenhanced image well depicts two calcifications in the lymph node and aorta. The calcification in the lymph node became blurred probably due to noise. **(c)** On enhanced weighted average image, the calcification in the lymph node is not visible due to enhancement.

Figure 7

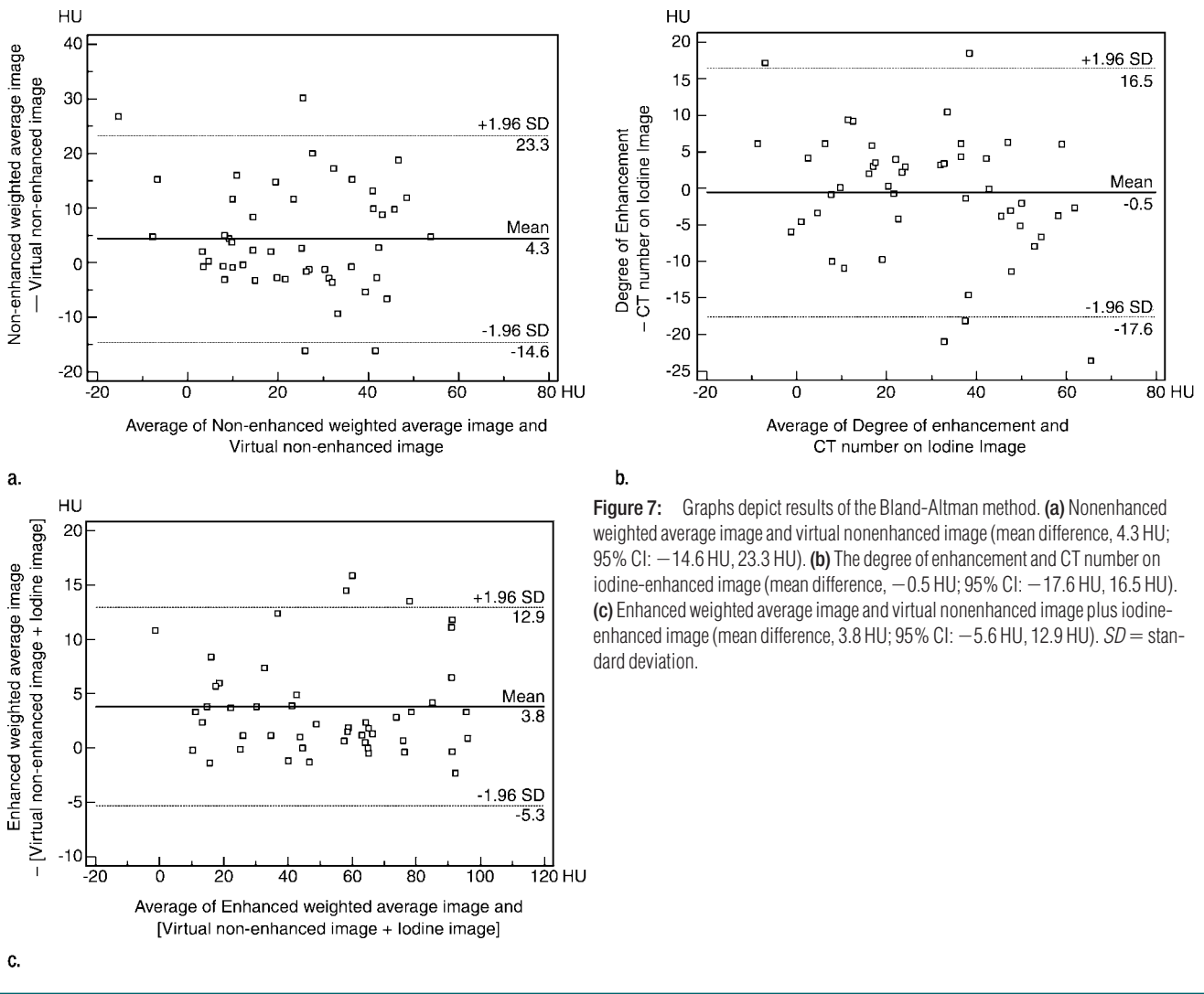


Figure 7: Graphs depict results of the Bland-Altman method. **(a)** Nonenhanced weighted average image and virtual nonenhanced image (mean difference, 4.3 HU; 95% CI: -14.6 HU, 23.3 HU). **(b)** The degree of enhancement and CT number on iodine-enhanced image (mean difference, -0.5 HU; 95% CI: -17.6 HU, 16.5 HU). **(c)** Enhanced weighted average image and virtual nonenhanced image plus iodine-enhanced image (mean difference, 3.8 HU; 95% CI: -5.6 HU, 12.9 HU). *SD* = standard deviation.

the degree of enhancement of SPN after iodine contrast agent administration has proved to be helpful for distinguishing malignant nodules from benign nodules at contrast-enhanced dynamic CT (3–9). However, contrast-enhanced dynamic CT has the disadvantage of an increased radiation dose to patients and of inaccurate measurement due to the different positioning of the ROI in the SPN on the serial images of dynamic scanning. A DE CT simultaneously provides virtual nonenhanced image and an iodine-enhanced image from a single scanning; therefore, we can acquire the CT number on a nonenhanced image and the iodine value in the SPN from

Table 1

Comparison of the Measurement of Enhancement

Analyzed Data	Malignant Nodules (n = 25)	Benign Nodules (n = 20)	P Value
CT number on iodine-enhanced image (HU)	36.5 ± 16.0	17.3 ± 21.8	.001
Degree of enhancement (HU)	37.0 ± 14.6	17.0 ± 17.9	<.001

Note.—Data are mean ± standard deviation.

the same ROI. This technique may prevent a nonenhanced scan as baseline study for dynamic enhancement study of nodules and it may also reduce mea-

surement error due to different positioning of the ROI on sequential images. Effect on measurement error might be more important in the relatively smaller

nodules. A single, enhanced CT scanning using DE provides additional information about the degree of enhancement of an SPN without additional radiation exposure.

In our study, there was a tendency for the sum of the CT numbers on virtual nonenhanced image and on iodine-enhanced image to be smaller than the CT number on enhanced weighted average image. Theoretically, the sum of CT numbers of those two calculated images has to be the same as the CT number on enhanced weighted average image when the DE technique is used to decompose enhanced structures into soft tissue and iodine. However, this is only valid as long as virtual nonenhanced, iodine-enhanced, and enhanced weighted average images are derived for the same volume; in reality, virtual nonenhanced image and iodine-enhanced image include a slightly larger volume due to filtering before material decomposition. Therefore, this effect may be caused by partial volume effects with air that were larger after application of the filtering.

Results of the Bland-Altman method and the ICC showed that the degree of enhancement and the iodine-enhanced image have a stronger agreement than do nonenhanced weighted average and virtual nonenhanced images. Moreover, the standard deviation of the degree of enhancement minus iodine-enhanced image is smaller than the standard deviation of nonenhanced weighted average image minus virtual nonenhanced image. This should not happen if an enhanced weighted average image is equivalent to virtual nonenhanced image plus iodine-enhanced image, but can again be explained by partial volume effects with air. In general, partial volume effects with air will have a bigger effect on virtual nonenhanced image

than on iodine-enhanced image, as the resulting shift of the CT numbers in the 80-kV versus 140-kV diagram is almost parallel to the difference vector between soft tissue and fat. The lower influence of partial volume effects on the iodine-enhanced image is beneficial for practice, because the CT number on the iodine-enhanced image and not on the virtual nonenhanced image is of interest, that is, is used for evaluating tumor vascularity. In principle, the CT numbers on virtual nonenhanced and iodine-enhanced images are expected to have larger systematic errors than the CT numbers on nonenhanced weighted average and enhanced weighted average images, because the material decomposition is sensitive to systematic errors on the 80-kV image, which—in comparison with the 140-kV image—is more affected by beam hardening artifacts and artifacts due to cross-scattered radiation. However, in reality, the error on iodine-enhanced image seems to be of similar magnitude or smaller than the error on the measurement of enhanced weighted average image minus nonenhanced weighted average image, which results from enhanced weighted average image and nonenhanced weighted average image being measured at two different ROIs. We evaluated the agreement by two ways: the Bland-Altman method and the ICC. Although there was some mismatch between the results of the two methods, the overall agreement was good. Moreover, in terms of diagnostic accuracy for malignancy, the CT number on the iodine-enhanced image showed a comparable result with the real degree of enhancement.

Demonstration of calcification on the virtual nonenhanced image, however, was not comparable to that on the nonenhanced weighted average image,

since most calcifications appeared smaller on virtual nonenhanced image than on nonenhanced weighted average image. Although most of the calcifications (93.8%) in the nodules and lymph nodes were detected on virtual nonenhanced image, some were not (6.2%). There are several reasons for this result: image noise of the virtual nonenhanced image is higher; the signal-to-noise ratio in the surface of calcifications is lower; the low-pass filter blurs the edges; and during material decomposition, the signal is lowered because part of the calcium is moved to the iodine image. Since presence of calcification in the lung nodules and lymph nodes implies benign etiology, differentiating calcification from contrast enhancement is important. However, some institutions, including our hospital, perform only enhanced scanning because of the relatively low benefit of a nonenhanced scanning, especially considering its double radiation dose. Enhancement of an SPN after iodine injection often obscures the presence of calcification in the nodule, especially if the calcification does not show substantially higher attenuation than the peak level of enhancement of the nodule. In this study protocol, we obtained 3-minute-delayed scans, as most malignant lung nodules show the peak level of enhancement at approximately 3 minutes (3.9). In our study, obscured calcifications on enhanced weighted average image were detected on virtual nonenhanced image in two patients. This result implies that a virtual nonenhanced image could be helpful when high attenuation is equivocal on an enhanced CT image. When high attenuation is suspected, we can retrospectively acquire a virtual nonenhanced image by means of postprocessing after CT by using DE.

The radiation dose of 1-minute-delayed scans covering the full thorax by using a DE CT was similar to that of scanning by using single-energy multidetector CT or dual-source CT without the DE mode. This result indicates that single scanning by using a DE mode of a dual-source CT saves the amount of radiation of an additional nonenhanced

Table 2

Comparison of the Diagnostic Accuracy for Malignancy with a Cutoff Value of 20 HU

Analyzed Data	Sensitivity (%)	Specificity (%)	Accuracy (%)
CT number on iodine-enhanced image	92.0 (52.2, 85.9)	70.0 (47.9, 85.7)	82.2 (56.5, 82.4)
Degree of enhancement	72.0 (73.9, 98.9)	70.0 (47.9, 85.7)	71.1 (68.4, 90.7)

Note.—Data in parentheses are 95% CIs.

scanning. In routine practice, optional reconstruction of a virtual nonenhanced image after DE CT scanning may replace the additional nonenhanced CT scan.

One of the limitations of dual-source CT was the 26-cm field of view of the smaller detector system, unlike the 50-cm field of view of the larger detector system (Fig 3e and 3f). The region inside the field of view of the smaller detector system can be decomposed. Because of the 26-cm field of view of the smaller detector system, the peripheral portion of the lower lung could not be covered in some of our subjects. Therefore, patients with a small nodule in the far periphery of the lower lungs cannot be scanned by using this protocol. In the present study, all lung nodules were located inside the field of view of the smaller detector.

Another limitation of our study was that only a small number of patients having an SPN with calcification were included, since most of our study patients were planning to undergo percutaneous needle aspiration due to the presence of a radiologically indeterminate nodule. Detected calcifications in our study were mostly in the lymph nodes. One of the limitations was the small number of patients, which demonstrates that further studies are needed to definitely establish the feasibility of the new tool. Therefore, this application awaits further investigation to deter-

mine its reliability for detecting calcification in an SPN.

In conclusion, we were able to successfully differentiate the iodine component from the enhanced soft tissue by using DE CT. Acquisition of virtual nonenhanced and iodine-enhanced images with DE CT may be a feasible tool for the measurement of the degree of enhancement.

Acknowledgments: We acknowledge Park Joo-Young for her technical assistance and also thank Bonnie Hami, MA, for her contribution and advice regarding the manuscript editing.

References

1. Johnson TR, Krauss B, Sedlmair M, et al. Material differentiation by dual energy CT: initial experience. *Eur Radiol* 2007;17:1510–1517.
2. Flohr TG, McCollough CH, Bruder H, et al. First performance evaluation of a dual-source CT (DSCT) system. *Eur Radiol* 2006;16:256–268.
3. Swensen SJ, Morin RL, Schueler BA, et al. Solitary pulmonary nodule: CT evaluation of enhancement with iodinated contrast material—a preliminary report. *Radiology* 1992;182:343–347.
4. Swensen SJ, Brown LR, Colby TV, Weaver AL. Pulmonary nodules: CT evaluation of enhancement with iodinated contrast material. *Radiology* 1995;194:393–398.
5. Yamashita K, Matsunobe S, Tsuda T, et al. Solitary pulmonary nodule: preliminary study of evaluation with incremental dynamic CT. *Radiology* 1995;194:399–405.
6. Swensen SJ, Brown LR, Colby TV, Weaver AL, Midthun DE. Lung nodule enhancement at CT: prospective findings. *Radiology* 1996;201:447–455.
7. Zhang M, Kono M. Solitary pulmonary nodules: evaluation of blood flow patterns with dynamic CT. *Radiology* 1997;205:471–478.
8. Swensen SJ, Viggiano RW, Midthun DE, et al. Lung nodule enhancement at CT: multicenter study. *Radiology* 2000;214:73–80.
9. Jeong YJ, Lee KS, Jeong SY, et al. Solitary pulmonary nodule: characterization with combined wash-in and washout features at dynamic multi-detector row CT. *Radiology* 2005;237:675–683.
10. Brooks RA. A quantitative theory of the Hounsfield unit and its application to dual energy scanning. *J Comput Assist Tomogr* 1977;1:487–493.
11. Kelcz F, Joseph PM, Hilal SK. Noise considerations in dual energy CT scanning. *Med Phys* 1979;6:418–425.
12. Kalender WA, Klotz E, Kostaridou L. An algorithm for noise suppression in dual energy CT material density images. *IEEE Trans Med Imaging* 1988;7:218–224.
13. Zatz LM. The effect of the kVp level on EMI values: selective imaging of various materials with different kVp settings. *Radiology* 1976;119:683–688.
14. Siegel MJ, Schmidt B, Bradley D, Suess C, Hildebolt C. Radiation dose and image quality in pediatric CT: effect of technical factors and phantom size and shape. *Radiology* 2004;233:515–522.
15. Medina LS, Zurakowski D. Measurement variability and confidence intervals in medicine: why should radiologists care? *Radiology* 2003;226:297–301.